MicroRNA-30 modulates metabolic inflammation by regulating Notch signaling in adipose tissue macrophages

Kathryn Miranda[1] · Xiaoming Yang[1] · Marpe Bam[1] · E. Angela Murphy[1] · Prakash S. Nagarkatti[1] · Mitzi Nagarkatti[1]

Abstract

Background/objectives: Obesity is a pandemic disorder that is characterized by accumulation of adipose tissue and chronic low-grade inflammation that is driven primarily by adipose tissue macrophages (ATMs). While ATM polarization from pro-(M1) to anti-(M2) inflammatory phenotype influences insulin sensitivity and energy expenditure, the mechanisms of such a switch are unclear. In the current study, we identified epigenetic pathways including microRNAs (miR) in ATMs that regulate obesity-induced inflammation.

Subjects/methods: Male C57BL/6J mice were fed normal chow diet (NCD) or high-fat diet (HFD) for 16 weeks to develop lean and diet-induced obese mice, respectively. Transcriptome microarrays, microRNA microarrays, and MeDIP-Seq were performed on ATMs isolated from visceral fat. Pathway analysis and bone marrow-derived macrophage (BMDM) transfections further allowed computational and functional analysis of miRNA-mediated ATM polarization.

Results: ATMs from HFD-fed mice were skewed toward M1 inflammatory phenotype. Concurrently, the expression of miRs 30a-5p, 30c-5p, and 30e-5p was downregulated in ATMs from HFD mice when compared to mice fed NCD. The miR-30 family was shown to target Delta-like-4, a Notch1 ligand, whose expression was increased in HFD ATMs. Inhibition of miR-30 in conditioned BMDM triggered Notch1 signaling, pro-inflammatory cytokine production, and M1 macrophage polarization. In addition, DNA hypermethylation was observed in *mir30*-associated CpG islands, suggesting that HFD downregulates miR-30 through epigenetic modifications.

Conclusions: HFD-induced obesity downregulates miR-30 by DNA methylation thereby inducing Notch1 signaling in ATMs and their polarization to M1 macrophages. These findings identify miR-30 as a regulator of pro-inflammatory ATM polarization and suggest that miR-30 manipulation could be a therapeutic target for obesity-induced inflammation.

Introduction

Overnutrition causes obesity and adipose tissue macrophage (ATM)-dependent inflammation that enhances risk for type II diabetes, cardiovascular disease, and some cancers. Macrophages are innate immune cells that display remarkable plasticity between pro- and anti-inflammatory

phenotypes. They are routinely classified as M1 and M2 respectively, although various subtypes exist [1]. At steady state, resident M2-like ATMs contribute to insulin sensitivity and adipose tissue homeostasis through production of anti-inflammatory cytokines, such as interleukin-10 [2]. During obesity, M1 ATMs dominate the adipose tissue in both phenotype and abundance, promoting insulin resistance and chronic low-grade inflammation [3]. Owing to vast disparities seen in ATM functionality between lean and obese individuals, ATMs have been suggested to play a substantial role in determining development of obesity-related pathologies. Therapeutic strategies that decrease ATM-dependent inflammation have been heavily investigated due to the tight correlation of macrophage-dependent inflammation and insulin resistance.

Notch signaling plays key roles in metabolic and inflammatory processes [4]. It is highly conserved juxtacrine signaling utilized by numerous cell types, including

✉ Mitzi Nagarkatti
mitzi.nagarkatti@uscmed.sc.edu

1 Department of Pathology, Microbiology and Immunology, University of South Carolina School of Medicine, Columbia, SC 29209, USA

macrophages and adipocytes. Binding of Notch receptors (Notch1–4) by Delta-like and Jagged ligands (DLL1, -3, -4 and JAG1, -2) initiates proteolytic release of the Notch intracellular domain allowing it to translocate to the nucleus and activate Jκ-recombination signal-binding protein (RBP-J)-dependent transcription [5]. In macrophages, Notch1 signaling promotes pro-inflammatory polarization through interferon regulatory factor 8 (IRF8) and nuclear factor-κB transcriptional pathways, whereas in adipocytes, Notch1 signaling inhibits white adipose tissue browning and energy expenditure and promotes insulin resistance [6–8]. Additionally, blockade of the canonical Notch1 ligand DLL4 improves atherosclerosis and metabolic disease indicating DLL4–Notch1 signaling is directly involved in the crosstalk of inflammatory and metabolic pathways [9].

Recent studies in our laboratory have identified epigenetic modifications that regulate immune responses in a variety of diseases, including post-traumatic stress disorder, multiple sclerosis, colitis, and liver failure [10–13]. MicroRNAs (miRNA, miR) are short (~22 nucleotide long) non-coding RNAs that posttranscriptionally inhibit protein translation by binding the 3' untranslated region (3'UTR) of target mRNAs [14]. Because approximately 60% of protein-coding genes are known conserved targets of miRNAs, they have emerged as important regulators of biological functions, such as immune system development and inflammatory responses [15, 16]. DNA methylation occurs when methyl groups are added to cytosines by DNA methyltransferases (DNMT). These methylated cytosines primarily reside in CpG islands near transcription start sites and repress gene transcription by blocking binding sites for transcription factors through chromatin condensation. Importantly, DNA methylation and miRNAs have been associated with development of aging-associated pathologies, including obesity, atherosclerosis, and cancer [17–19].

Numerous miRNAs have already been classified to regulate differentiation and function of both adipocytes and macrophages. However, characterization of miRNA expression specifically in ATMs from lean and obese individuals has not been previously reported. Such investigation warrants merit because ATMs comprise a unique cell type due to their immunometabolic functions and dominance in the adipose tissue of obese individuals. Also, ATMs are thought to be the main initiators of obesity-induced inflammation and insulin resistance [20]. In this report, we have identified dysregulated miRNAs in ATMs during obesity, which demonstrates that obese ATMs have distinct miRNA profiles that are likely to contribute to their inflammatory phenotype. Specifically, we discovered downregulation of the miR-30 family in ATMs to modulate macrophage phenotype. Our findings demonstrate that miR-30 regulates pro-inflammatory polarization of ATMs and is likely due to regulation of DLL4-mediated

Notch1 signaling. Our data also suggest therapeutic manipulation of this miRNA family or the epigenetic mechanisms that regulate its expression may constitute therapeutic modalities for obesity-induced inflammation, insulin resistance, and related cardiometabolic disorders.

Materials and methods

Mice

Six-to-8-week-old male and female C57Bl/6J mice and 22-week-old male C57Bl/6J mice fed either 60% kcal high-fat diet (HFD; D12492, Research Diets), normal chow diet (NCD; 8904, Envigo Teklad), or purified 10% low-fat diet (LFD, D12450J, Research Diets) where indicated for 16 weeks were obtained from The Jackson Laboratory and housed in a specific pathogen-free facility. Studies were not blinded and mice were not randomized into experimental groups. At the conclusion of each study, mice were euthanized by overdose isoflurane inhalation. All procedures were performed in accordance with protocols approved by the University of South Carolina Institutional Animal Care and Use Committee.

Analytical procedures

Body composition of lean mass and fat mass were measured by dual-energy X-ray absorptiometry (LUNAR PIXImus). Mice were placed under isoflurane anesthesia and scanned in the prone position with the head region being excluded. Body weight was monitored using an electronic gram scale with precision of ±0.1 g. For glucose tolerance tests (GTTs), mice underwent a 5 h morning fast before fasting glucose measurement and then gavaged with 2 g/kg lean mass glucose (Sigma G7528). Blood glucose was measured 15, 30, 60, and 120 min post-glucose bolus by applying approximately 5 μL tail-tip blood to a glucose test strip in a glucose meter (Contour Next, Bayer).

Adipose tissue dissociation and ATM isolation

To dissociate cells of the stromal vascular fraction (SVF), epididymal fat pads from 22-week-old mice were dissected, rinsed in phosphate-buffered saline (PBS), and homogenized in 5 mL digestion media consisting of Hank's Balanced Salt Solution containing 2% bovine serum albumin (BSA) and 1 mg/mL collagenase (Sigma C6885) using a GentleMACs dissociator (Miltenyi Biotec). An additional 5 mL digestion media was added to the homogenates and incubated at 37 °C, 75 RPM, 30–40 min until fully dissociated. Next, 5 mL complete Dulbecco's Modified Eagle's Medium and Ham's F-12 Nutrient Mixture

(DMEM/F12) containing 10% heat-inactivated fetal bovine serum (FBS) and 1% penicillin/streptomycin was added to the samples before filtering through a 100-μm nylon mesh. SVF cells were pelleted (1200 RPM, 4 °C, 10 m), red blood cell (RBC)-lysed, filtered through a 70-μm nylon mesh, and washed in complete DMEM/F12, then used immediately for desired application. To purify ATMs, SVF cells were washed twice in fluorescence-activated cell sorter (FACS) buffer consisting of PBS, 2% heat-inactivated FBS, and 1 mM EDTA, then incubated in FcR-Blocker (StemCell Tech, 18720) followed by phycoerythrin (PE)-conjugated anti-F4/80 (BioLegend, Clone BM8). F4/80+ cells were immunomagnetically selected by EasySep PE-positive selection kit according to the manufacturer's protocol including four total wash steps (StemCell Tech, 18557). Flow cytometry was used to verify selection purity, which was >85%.

RNA purification, cDNA synthesis, and quantitative reverse transcriptase polymerase chain reaction (qRT-PCR)

ATMs were lysed in Qiazol and total RNA was purified using the Qiagen miRNeasy Micro Kit. RNA concentration and purity was measured using a NanoDrop 2000 spectrophotometer. In all, 400 ng total RNA was reverse transcribed to cDNA using the Qiagen miScript II RT Kit with HiFlex buffer. To validate miRNA expression by qRT-PCR, miScript SYBR Green PCR Kit and miScript miRNA Primer Assays were used (Qiagen).

ATM miRNA and transcriptome microarrays

MicroRNA and transcriptome microarrays were performed using three biological replicates of total RNA isolated from pools of ATMs (NCD: pools of 20 mice, HFD: pools of 10 mice). For each miRNA microarray, 500 ng total RNA was polyadenylated and then labeled using the Affymetrix FlashTag Biotin HSR RNA Labeling Kit. Labeled samples were hybridized to Affymetrix miRNA 4.0 chips overnight (16 h, 48 °C, 60 RPM) then washed, stained, and scanned on an Affymetrix GCS 3000 system following the manufacturer's protocols. For transcriptome microarrays, 100 ng total RNA was used as starting material. RNA was prepared for hybridization by using the Affymetrix GeneChip WT PLUS Reagent Kit according to manufacturer's protocol. Labeled samples were hybridized to MTA 1.0 chips overnight (16 h, 45 °C, 60 RPM) then washed, stained, and scanned on an Affymetrix GCS 3000 system. Affymetrix Expression Console Version 1.4.1.46 was used for quality control, data summarization, and normalization. Affymetrix Transcriptome Analysis Console Version 3.1.0.5 was used to perform differential expression analyses. Transcripts or miRNAs were considered differentially expressed between the two groups if linear fold change (FC) was >±2 and the analysis of variance (ANOVA) p-value was <0.05. Heatmap figures of differentially expressed miRNAs and mRNAs were made using Genesis Version 1.7.7. [21]

Immunofluorescence

Epididymal fat was dissected, minced (~3 × 3 mm^2), washed in PBS, and then fixed in 4% paraformaldehyde for 3 h. Fixed tissues were permeabilized with 1% Triton X-100 for 10 min and then blocked with 1% BSA and FcR-Blocker for 1 h at room temperature (RT). Samples were incubated with primary antibody (BioLegend: anti-F4/80-AlexaFluor488 clone: BM8, and anti-Notch1 clone: HMN1-12, or anti-DLL4 clone: HMD4-1) overnight at 4 °C and then incubated with anti-Hamster IgG-AlexaFluor633 secondary antibody for 1 h at RT (Invitrogen SA1-26817, Molecular Probes Labeling Kit A20170). Tissues were counterstained with 40 μM Hoechst 33342 and 5 μM BODIPY 558/568 C12 (Molecular Probes H21492 & D3835) for 1 h at RT, then washed and mounted on slides using a Vaseline boundary and Fluoromount-G (eBioscience, 00-4958-02).

Confocal microscopy and image analysis

Confocal images of whole-mount adipose tissue were acquired on a Zeiss LSM 510 Meta Confocal Scanning Laser Microscope equipped with ultraviolet, Argon, green HeNe, and red HeNe lasers. Five random images per sample were taken using a 40× water immersion objective. Original.lsm files were imported into Fiji (Fiji Is Just ImageJ, NIH) and then split into channels. Thresholds were applied to the Cy5 channel using Fiji's max Entropy algorithm to identify regions of interest (ROIs) that express either Notch1 or DLL4. Area and intensity (mean gray value) were measured for each ROI. The product of positive signal area and intensity were used to determine total expression per image. Each biological replicate is the mean expression of five images. We then divided the expression values for each biological replicate by the mean of the NCD biological replicates. Therefore, data are presented as fold expression in arbitrary units with mean NCD set as control.

Flow cytometry

Freshly isolated SVF cells or cultured bone marrow-derived macrophages (BMDMs) were washed in FACS buffer and then incubated on ice with FcR-Blocker for 10 min followed by appropriate fluorochrome-conjugated antibodies or isotype controls (BioLegend, anti-CD11b-AlexaFluor488 clone: M1/70, anti-F4/80-PE clone: BM8, anti-DLL4-APC clone: HMD4-1, anti-CD45-PECy7 clone: 30-F11, anti-

CD11c-APC clone: N418) for 50 min. Stained cells were washed 3× in FACS buffer and then analyzed on a Beckman Coulter FC500 or BD FACSCelesta flow cytometer. Plots were analyzed with the Beckman Coulter CXP Software or FlowJo v10.

In vitro locked nucleic acid (LNA) transfection assays

BMDMs were differentiated from bone marrow cells (BMC) by flushing the tibia and femur of 6–8-week-old female C57Bl/6J mice with PBS. BMCs were filtered through a 70-µm nylon mesh, RBC-lysed, washed, and then cultured in complete DMEM/F12 supplemented with 10% FBS, 1% penicillin/streptomycin, 2 mM L-glutamine, and 1 U/mL M-CSF (BioLegend, 576406) for 7–10 days. 3T3-L1 adipocyte-conditioned media (CM-3T3-L1A) was generated by differentiating 3T3-L1 preadipocytes into adipocytes according to Zen-Bio 3T3-L1 Adipocyte Care Manual (ZBM0009.03). Preadipocyte medium, differentiation medium, and adipocyte maintenance medium were also used (Zen-Bio, PM-1-L1, DM-2-L1, AM-1-L1). Conditioned medium was collected between days 7 and 14 post-differentiation, 0.22-µm filtered, aliquoted, and stored at $-80\,°C$ until use. For transfection assays, mature BMDMs were plated in poly-D-lysine-coated six-well plates at a density of 5×10^5 cells in 2 ml CM-3T3-L1A containing 10% FBS without antibiotics. BMDMs were incubated 24 h (37 °C, 5% CO_2, 95% humidity) before transfection. Transfection complexes were prepared by diluting Lipofectamine3000 and LNA in Opti-MEM to final concentrations of 2% (v/v) and 0.32 µM, respectively. Mixtures were incubated for 15–20 min at RT to allow complexes to form. Meanwhile, conditioned BMDMs were washed 3× in pre-warmed Dulbecco's PBS (DPBS), and then media was replaced with 2 mL Opti-MEM. Next, 500 µL transfection complexes were added drop-wise to each well. Cells were incubated (37 °C, 5% CO_2, 95% humidity) for 5–6 h to allow LNA uptake, washed 3× in pre-warmed DPBS, then media replaced with DMEM/F12 containing 10% FBS, 1% penicillin/streptomycin, and 2 mM L-glutamine, and cultured for an additional 18 h. For inhibition studies, N-S-phenyl-glycine-t-butyl ester (DAPT; 5 µM), anti-DLL4 antibody (1 µg/mL), or appropriate vehicle/isotype antibody controls were added to the culture media. MirCURY LNA oligonucleotides were obtained from Exiqon (LNA Sequences—Ctr LNA: TAACACGTCTA-TACGCCCA, Anti-30a: TTCCAGTCGAGGATGTTTAC, Anti-30c: CTGAGAGTGTAGGATGTT, Anti-30e: TCCAGTCAAGGATGTTTAC).

Protein extraction and western blotting

Cultured BMDMs were washed twice in ice-cold PBS, then directly scrapped into 100 µL blue loading buffer (Cell Signaling Technology 7722) and kept on ice. Protein lysates were sonicated for 10 s, then heated at 95 °C for 5 min before loading 20 µL on Mini-Protean TGX Protein Gels (BioRad 4569034). Precision Plus Protein Dual Color Standards (BioRad 1610374) were loaded for a molecular weight ladder. Samples were run at 40 V for 30 min followed by 80 V for 1.5 h. Proteins were transferred to nitrocellulose membranes by using iBlot2 NC stacks and the ThermoFisher iBlot2 western transfer system running the P0 protocol (20 V for 1 min, 23 V for 4 min, then 25 V for 2 min). Membranes were blocked in 5% dry milk or 5% BSA for 1 h and then washed 3× in Tris-buffered saline containing 0.1% Tween-20 (TBS-T). Membranes were incubated in primary antibody overnight at 4 °C with gentle shaking and then washed 3× for 5 min in TBS-T. Membranes were incubated in secondary antibody for 1 h at RT, and then washed 3× for 5 min in TBS-T before addition of ECL substrate and exposure to X-ray film. Films were scanned and densitometry measurements were made using ImageJ gel analysis features (NIH).

Enzyme-linked immunosorbent assays (ELISA)

Culture supernatants were aspirated and centrifuged at 5000 RPM, 5 min, 4 °C to rid of debris, then aliquoted and stored $-80\,°C$ before assaying. DLL4 ELISA kits were purchased from Abcam (ab213860). Mouse tumor necrosis factor-α (TNFα) and C-C chemokine motif ligand 2 (CCL2) ELISA kits were purchased from BioLegend (TNFα 530901 & CCL2 432701). Assays were performed according to the manufacturers' protocols and plates were read at 450 nm. Concentrations were calculated using standard curves.

Methylated DNA immunoprecipitation sequencing (MeDIP-Seq)

MeDIP-Seq libraries were generated from ATM DNA as previously described and sequenced with single-end reads of 75 bp on an Illumina NextSeq500 [22]. Data analysis was performed as previously described [22]. Mapped reads were analyzed using the MEDIPS software [23]. Peaks were visualized in the Integrated Genome Browser [24]. The UCSC genome browser was used to locate CpG islands within 10 kb of miR-30 gene-coding regions [25].

Methylation-specific PCR

Genomic DNA from NCD and HFD ATMs were isolated using the Qiagen AllPrep DNA/RNA/miRNA Universal Kit (80224). Bisulfite conversion of DNA was performed using the Qiagen EpiTect Fast DNA Bisulfite Kit (59824). PCR using methylated and unmethylated primers specific for the
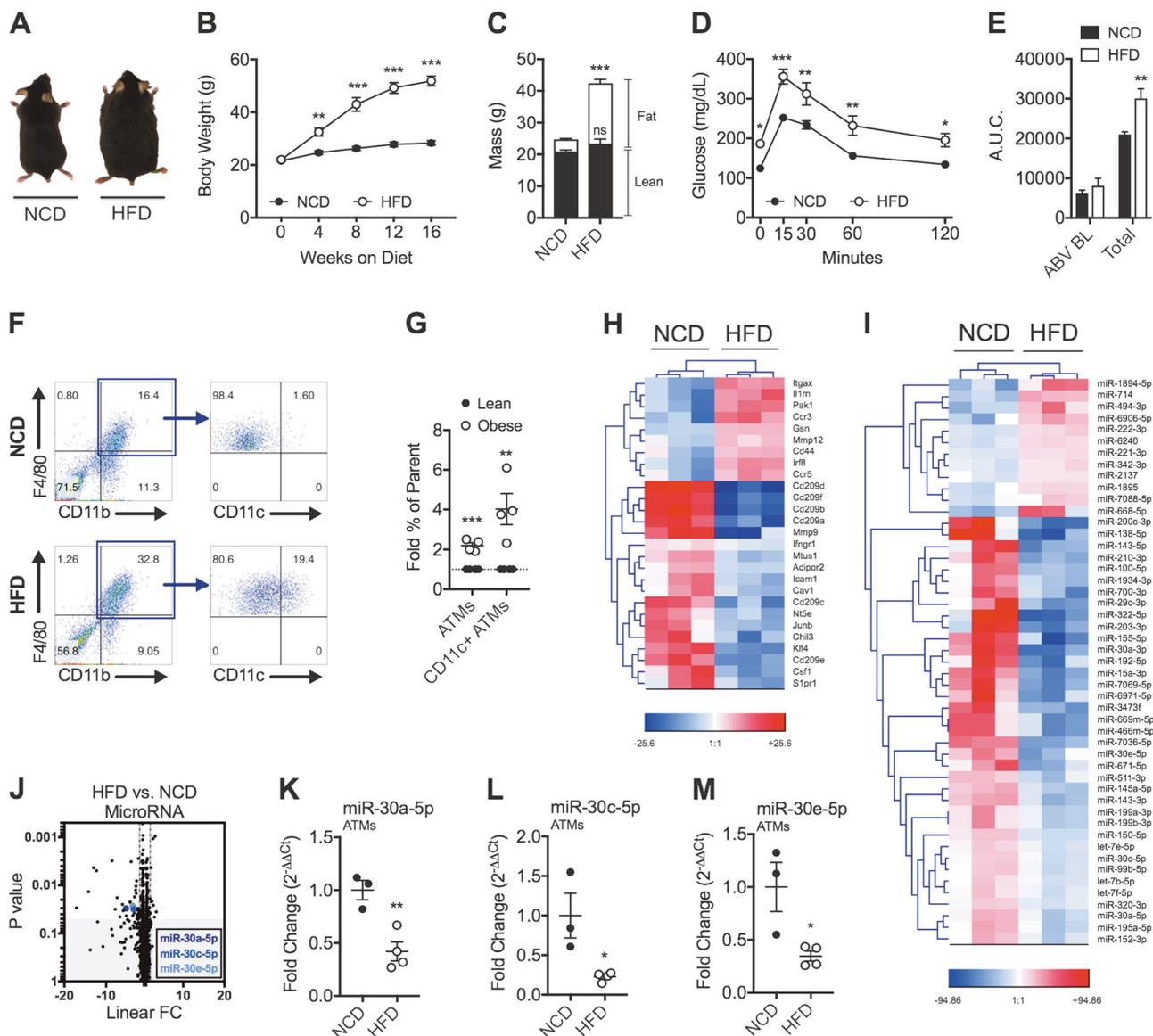
Fig. 1 HFD-induced obesity stimulates ATM inflammation and miRNA dysregulation. To study HFD-induced obesity, male C57BL/6J mice were fed NCD or HFD for 16 weeks until aged 22 weeks. **a** Representative photo of mice after 16 weeks of NCD or HFD feeding. **b** Weekly measurements of body weight growth. **c** DEXA body composition after 16 weeks of diet. **d** Oral glucose tolerance test (GTT) after 16 weeks of diet. **e** Area under the curve (A.U.C.) for GTT. Represented are A.U.C. above baseline (ABV BL) or total A.U.C. **f** Flow cytometric dot plots of F4/80$^+$/CD11b$^+$/CD11c$^+$ ATMs in the epididymal fat stromal vascular fraction (SVF) of NCD- or HFD-fed mice. **g** Fold percentage increase quantification of F4/80$^+$/CD11b$^+$ cells in the SVF (denoted as "ATMs") and CD11c$^+$ ATMs. Lean mice were fed either NCD or 10% low-fat diet (LFD). Obese mice were fed 60% HFD. **h–j** Pooled F4/80+ ATMs from epididymal fat were used for transcriptome and miRNA microarrays. **h** Transcriptome microarray heatmap of differentially expressed mRNAs in ATMs related to macrophage polarization. **i** MicroRNA heatmap of differentially expressed miRNAs in ATMs. **j** MicroRNA array volcano plot depicting linear fold change (FC) vs. ANOVA p-value significance. **k–m** qRT-PCR expression validation of miRs 30a-5p, 30c-5p, and 30e-5p. For **a–f**, the values are shown as mean ± SEM and are from a single experiment representative of at least three independent experiments with five mice per experimental group. For **g**, data are shown as mean ± SEM of four independent experiments with five mice per experimental group. For **h–m**, the data shown are mean ± SEM and are from 3–4 independent experiments with 20 pooled NCD mice and 10 pooled HFD mice per experiment. Statistical differences were determined by using Student's t-test. *$p < 0.05$, **$p < 0.01$, ***$p < 0.001$. See also Figure S1 and Table S1

Nfyc CpG island (Methylated: Fwd—TTCGTTAATGG-GAGAAAGTTC, Rev—CTACCGCCGCCATATTATA; Unmethylated: Fwd—TTTTTTGTTAATGGGAGAAAGT TT, Rev—ACTCTACCACCACCATATTATA). Primers were designed using the ThermoFisher Methyl Primer Express Software v1.0. BioRad iQ SYBR Green Supermix was used and qRT-PCR was run using the following reaction conditions: initial denaturation—95 °C 5 m followed by 31

cycles at 95 °C 15 s, 49.8 °C 30 s, and 70 °C 35 s. PCR products were run on a 1.5% agarose gel and bands were quantified using FIJI gel analysis features. Methylation ratio was determined by dividing methylated by unmethylated quantities (M/U).

Statistical analysis

Statistical analyses were performed using GraphPad Prism Version 7.000 for Mac, GraphPad Software, La Jolla, CA, USA, www.graphpad.com. Values are expressed as mean ± standard error. Two-tailed Student's t-tests were performed for paired analyses. One-way ANOVA with a Bonferroni post hoc correction were used for multiple group analyses. The null hypothesis was rejected if $p < 0.05$. All experiments were repeated at least twice, unless otherwise indicated in each figure legend. Detailed sample sizes are provided in each figure legend. Sample sizes were chosen by power analysis based on pilot studies.

Results

Obesity promotes ATM miRNA dysregulation and pro-inflammatory phenotype

To study ATMs associated with obesity (will be referred to as obese ATMs), we used a HFD-induced obesity model whereby 6-week-old male C57BL/6J mice were fed HFD or NCD for 16 weeks to generate diet-induced obese and lean control mice. HFD-fed mice more than doubled their body weight during 16 weeks of feeding, whereas NCD-fed mice increased their weight by ~3% (Fig. 1a–c), and HFD-induced weight gain occurred due to selective increases in fat mass (Fig. 1c). As expected, HFD also caused glucose intolerance measured by GTT (Fig. 1d,e).

While phenotyping ATMs, we observed percentages of ATMs (F4/80$^+$/CD11b$^+$) and CD11c$^+$ ATMs in epididymal fat of obese mice were more than two- and four-fold that of lean mice, respectively (Fig. 1f, g). To identify gene expression alterations in HFD and NCD ATMs, we performed transcriptome microarrays using F4/80+ cells from epididymal fat of HFD and NCD mice. Principal component analysis (PCA) displayed that HFD and NCD ATMs have distinct transcript expression profiles (Supplemental Fig. 1A). HFD ATMs exhibited increased M1-associated and decreased M2-associated gene expression (Fig. 1h). Notably, Irf8, which encodes a transcription factor activated by Notch-RBPJ signaling, as well as Itgax, which encodes the M1 surface marker CD11c, were upregulated in obese ATMs [3, 8]. Alternatively, Klf4, which encodes Krüppel-like factor 4 that cooperates with signal transducer and activator of transcription factor 6 to promote M2

polarization, and Adipor2, which encodes a receptor for the anti-inflammatory adipokine adiponectin, were downregulated in obese ATMs [26, 27]. Together these observations suggested that HFD ATM phenotype was skewed toward M1.

To identify differentially expressed miRNAs in ATMs during obesity, we performed miRNA microarrays using F4/80+ cells isolated from epididymal fat of HFD and NCD mice. PCA showed HFD and NCD ATMs have distinct miRNA expression profiles (Supplemental Fig. 1B). In total, there were 37 downregulated and 12 upregulated miRNAs in HFD vs. NCD ATMs (Fig. 1i, j). Additionally, transcriptome microarrays showed that there were 946 downregulated and 920 upregulated transcripts in HFD vs. NCD ATMs. Of these, 216 and 273 coding genes were upregulated and downregulated, respectively (Supplemental Fig. 1C). We performed core analysis on these dysregulated miRNAs and transcripts using Qiagen Ingenuity Pathway Analysis and observed significant overlap with canonical pathways, including hepatic fibrosis and atherosclerosis signaling, disorders such as cancer and hepatic disease, cellular functions including movement and survival, and toxic effects including cardiotoxicity, hepatotoxicity, and nephrotoxicity (Supplemental Figs. 1D-1H).

Upon closer examination of dysregulated miRNAs during obesity, we observed downregulation of miR-322-5p (−17.1 linear FC) and miR-155-5p (−14.19 linear FC), which have been previously characterized for their involvement in macrophage functions [28, 29]. Interestingly, we also noted downregulation of miRs -30a-5p, -30c-5p, and -30e-5p in HFD ATMs (−12.27 combined linear FC) when compared to NCD ATMs, thereby indicating that the miR-30 family may play a role in macrophage polarization (Fig. 1i–m).

The miR-30 target DLL4 is associated with ATM inflammation

When we looked at potential target molecules for miR-30, we found through in silico analyses that it may target the 3'UTR of Dll4 (Supplemental Fig. 2a-c). Previous studies had confirmed miR-30-Dll4 targeting using luciferase reporter assay [30, 31]. Interestingly, DLL4 has been shown to be involved in Notch signaling [9, 32, 33]. To that end, we evaluated the expression of Notch1 and the miR-30 target DLL4 in adipose tissue. Notch1 and DLL4 were visualized in whole-mounted epididymal fat by confocal microscopy (Fig. 2a, c). Adipose tissue expression of DLL4 but not of Notch1 was elevated in HFD-fed mice (Fig. 2b, d). Flow cytometric analysis of epididymal fat SVFs was then used to confirm that DLL4 expression was elevated on ATMs (CD45$^+$/CD11b$^+$/F4/80$^+$/DLL4$^+$) (Fig. 2e, f). Specifically, elevated DLL4 expression was most pronounced
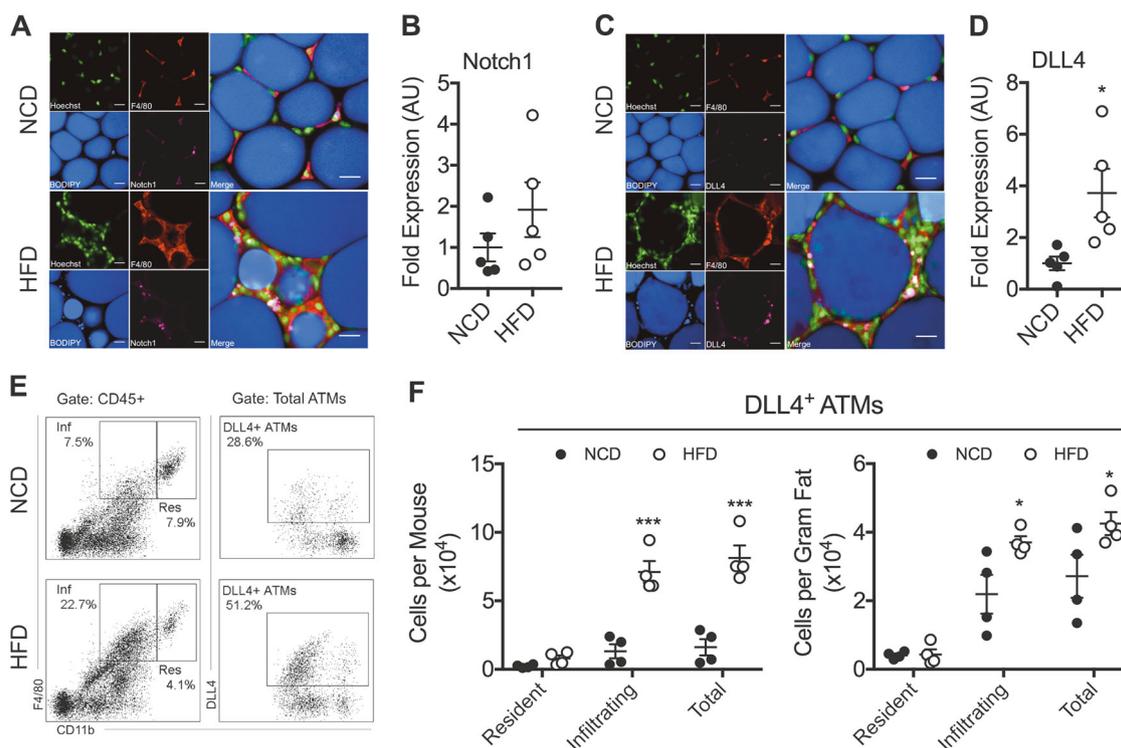
Fig. 2 DLL4 expression is elevated in obese ATMs. HFD-induced obesity was studied as described in Fig. 1 legend. At age 22 weeks-old, visceral adipose tissue and adipose SVFs were analyzed for DLL4 expression. **a**, **c** Immunofluorescent staining of whole-mount epididymal fat. Scale bar = 20 μm. Presented are representative confocal micrographs of Notch1 (**a**) or DLL4 (**c**). **b**, **d** Image quantification of Notch1 (**b**) or DLL4 (**d**) in adipose tissue. The values are shown as mean ± SEM and are from. single experiment representative of two independent experiments with five mice per experimental group.
e Flow cytometry dot plots of DLL4$^+$ ATMs in epididymal fat. CD11b^{int} are denoted as infiltrating ("Inf") and CD11b^{hi} are denoted as resident ("Res"). **f** Quantification of DLL4$^+$ ATM cell counts represented per mouse and per gram fat. Values are presented as mean ± SEM and are from a single experiment representative of two independent experiments with four biological replicates (pools of 1–6 mice) per experimental group. Statistical significance was determined by Student's t-test. *$p < 0.05$, ***$p < 0.001$. See also Figure S2

in the CD45$^+$/CD11b^{int}/F4/80$^+$ subset of infiltrating ATMs (Fig. 2f).

MicroRNA-30 inhibition promotes DLL4–Notch signaling-induced inflammation in macrophages

To further demonstrate involvement of miR-30 in regulation of DLL4-mediated Notch signaling and pro-inflammatory response in macrophages, we developed an in vitro assay to mimic the downregulated miR-30 expression observed in vivo in obese ATMs. To that end, naive BMDMs were cultured in conditioned medium from differentiated 3T3-L1 adipocytes (CM-3T3-L1A) to confer an ATM-like phenotype and then transfected with miRNA inhibitor LNA, which targeted miRs-30a-5p (Anti-30a), -30c-5p (Anti-30c), and -30e-5p (Anti-30e) (Fig. 3a). BMDMs transfected with Anti-30a, Anti-30c, and Anti-30e LNAs had decreased expression of miRs -30a-5p, -30c-5p, and -30e-5p relative to Mock and control LNA (Ctr LNA)-transfected controls, although the inhibitors displayed some cross-reactivity (Supplemental Fig. 3). Anti-30a, Anti-30c, and Anti-30e

transfection increased DLL4 and activated Notch1 intracellular domain (N1ICD) expression compared to Mock and Ctr LNA (Fig. 3b, c). Pro-inflammatory cytokines TNFα and CCL2 were also elevated in culture supernatants of inhibitor-transfected cells (Fig. 3d, e). Moreover, miR-30 inhibitors promoted increased surface expression of CD11c (Fig. 3f, g). Treatment of transfected cells with the Notch/γ-secretase inhibitor DAPT reduced induction of CD11c in miR-30 inhibitor-transfected cells (Supplemental Fig. 4B). Specific blockade of DLL4 signaling using anti-DLL4 antibody also reduced induction of pro-inflammatory cytokines TNFα and CCL2 in miR-30 inhibitor-transfected cells (Supplemental Figs. 4C & 4D). Conversely, lentiviral overexpression of miR-30a-5p in the RAW264.7 macrophage cell line reduced M1 polarization evidenced by decreased expression of CD11c and decreased TNFα and CCL2 production (Supplementary Figure 5). Together these data demonstrated that miR-30 plays an anti-inflammatory role in macrophages by regulating DLL4–Notch1 signaling, M1 polarization, and pro-inflammatory cytokine production in macrophages.
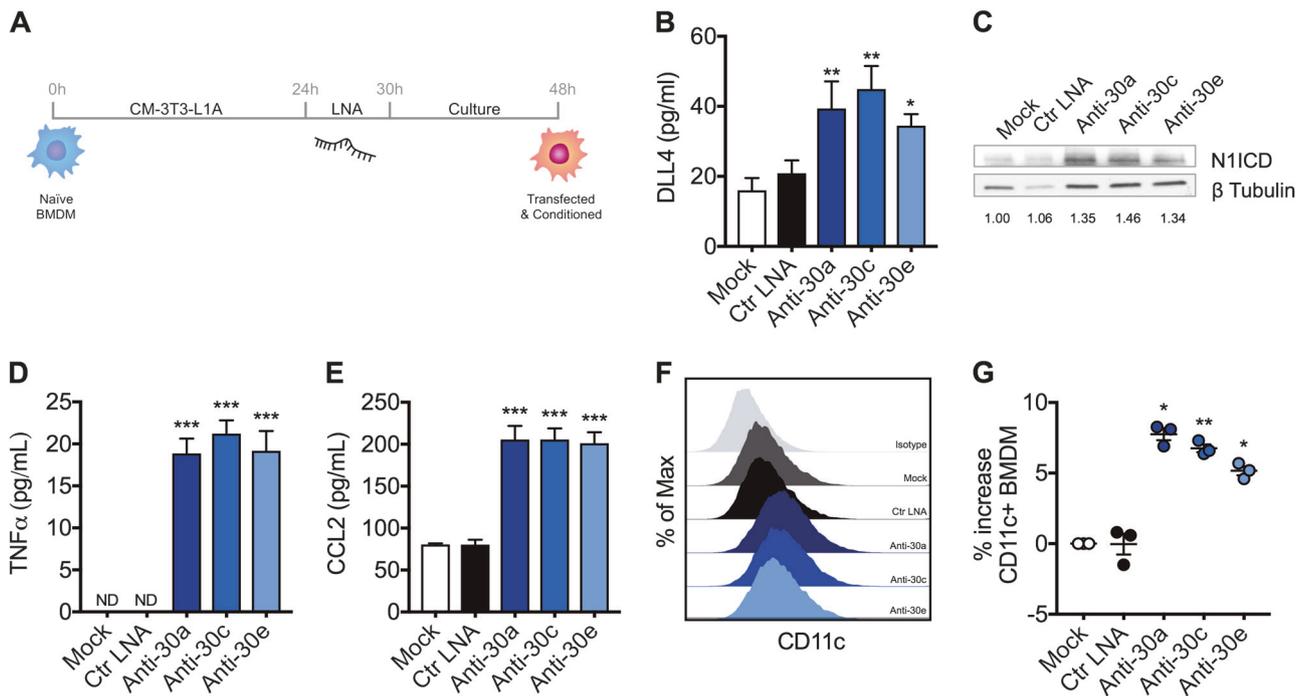
Fig. 3 miR-30 inhibition induces DLL4–Notch1 signaling and M1 polarization. BMDMs were differentiated from the bone marrow of normal mice and then used to study in vitro consequences of miR-30 inhibition on Notch signaling and macrophage polarization. **a** Schematic of in vitro experimental timeline. Differentiated BMDMs were incubated in CM-3T3-L1A prior to transfection with microRNA inhibitor LNA and subsequent culture. Cells and supernatants were harvested at 48 h. **b** DLL4 detected in culture supernatants by ELISA. **c** Western blot of cleaved/activated Notch1 (N1ICD). Fold induction relative to Mock is represented below each lane. **d**, **e** Pro-inflammatory cytokines TNFα (**d**) and CCL2 (**e**) detected in culture supernatants by ELISAs. **f** Flow cytometric histograms of CD11c expression in transfected BMDMs. **g** Percentage increase in CD11c+ macrophages. For **b**–**f**, values are presented as mean ± SEM and are from a single experiment representative of 2–3 independent experiments. For **e**, data presented are mean ± SEM of three independent experiments. Statistical significance was determined by one-way ANOVA with Bonferroni post hoc correction. *$p < 0.05$, **$p < 0.01$, ***$p < 0.001$ vs. Mock. See also Figures S3-S5
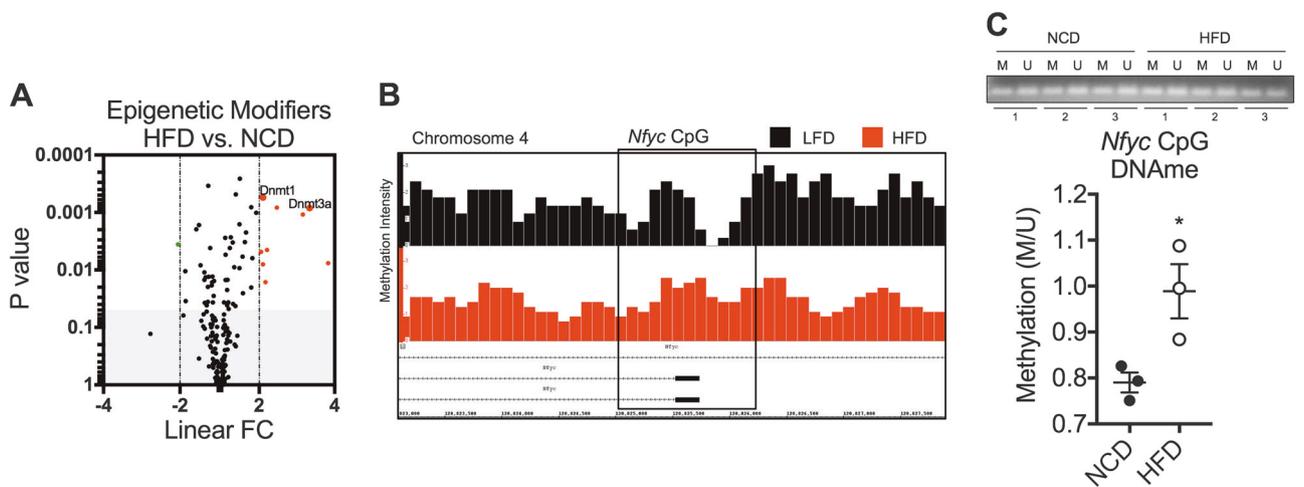

Fig. 4 DNA methylation-dependent regulation of miR-30. As shown in Fig. 1, F4/80+ ATMs were isolated from epididymal fat of 22-week-old HFD-induced obese and lean mice. Gene expression and DNA methylation were evaluated in ATMs. **a** Volcano plot displaying linear FC of genes encoding epigenetic modification enzymes and factors. Fold change and p-value observations were extracted from transcriptome microarrays (See Fig. 1 and Figure S1). **b** IGB visualization of MeDIP-Seq peak intensity of DNA methylation in the Nfyc promoter CpG island. **c** Methylation-specific PCR quantification of DNA methylation (DNAme) in the Nfyc promoter CpG island. For **a**, **c**, values presented are representative of 3 independent experiments with 20 pooled NCD mice and 10 pooled HFD mice per experiment. For **b**, data are representative of one experiment of 60 pooled LFD and 30 pooled HFD mice. Statistical differences were determined by using Student's t-test. *$p < 0.05$

Evidence for DNA methylation-dependent regulation of miR-30

Epigenetic modifications can occur due to various environmental factors such as stress, aging, and diet. Because this study involved diet-induced obesity, we investigated epigenetic mechanisms that may control miR-30 expression in ATMs. Data from transcriptome microarrays enriched for epigenetic modification enzymes and factors revealed that gene expression of *Dnmt1* and *Dnmt3a* were upregulated in ATMs of HFD vs. NCD-fed mice (Fig. 4a). Therefore, we investigated DNA methylation intensity of miR-30 gene regions. *Mir30c-1* and *mir30e* are located within the same intron of the *Nfyc* gene, which contains a CpG island in its promoter region. *Mir30a* and *mir30c-2* are intergenic miRNA genes that do not have any nearby CpG islands, therefore we were not able to identify DNA methylation as a potential epigenetic mechanism regulating their expression. We performed MeDIP-Seq to screen genome-wide DNA methylation in ATMs and found DNA hypermethylation in the *Nfyc*-promoter CpG island in HFD- vs. LFD-ATMs, indicating that the expression of miRs -30c and -30e may be regulated by DNA methylation. This was validated in NCD- and HFD-ATMs by methylation-specific PCR (Fig. 4c). Together, these data indicated DNA methylation-dependent downregulation of miR-30 may promote pro-inflammatory polarization of ATMs during obesity.

Discussion

There is a clear association between pro-inflammatory ATM polarization and insulin resistance during HFD-induced obesity. However, miRNA-mediated epigenetic mechanisms regulating ATM phenotype have not been well characterized. Our results unveil a role for the miR-30 family in modulating polarization of macrophages in visceral adipose tissue through regulation of the Notch1 ligand DLL4. Furthermore, we identified that DNA methylation may play a role in attenuating miR-30 expression. Jointly, these findings suggest important roles for miRNAs and DNA methylation in regulation of ATM polarization and obesity-induced insulin resistance.

DLL4 is a canonical Notch1 ligand that is linked to macrophage inflammation and metabolic disorders. DLL4 promotes M1 macrophage polarization [32, 33]. Blockade of DLL4 by administration of anti-DLL4 antibody in mice attenuates atherosclerosis and metabolic disease by decreasing macrophage infiltration and inflammatory response [9]. Interestingly, Notch signaling is also linked to insulin resistance [6, 7]. Conditional knockout of Notch1 or its downstream transcription factor RBP-J in adipocytes

ameliorates obesity and insulin resistance by promoting white adipose tissue browning and energy expenditure in mice [6]. These findings suggest that downregulation of the DLL4–Notch1 axis may hold significant therapeutic potential for various inflammatory and metabolic disorders. Furthermore, identification of regulatory mechanisms controlling this pathway could reveal therapeutic targets for cardiometabolic disorders. In the current study, we identified epigenetic regulatory mechanisms of this pathway in ATMs.

Growing bodies of evidence suggest that miRNA dysregulation and aberrant DNA methylation play pathogenic roles in clinical disorders, such as type II diabetes, atherosclerosis, and cancer. Inflammation is many times the underlying cause for these chronic diseases, and macrophages are key mediators of chronic inflammation. Additionally, obesity is well known to greatly increase risk for these diseases. Because ATMs are a primary source of pro-inflammatory cytokines that initiate chronic subclinical inflammation during obesity, ATMs contribute to progression toward comorbid diseases. In the current study, we observed increased infiltration and pro-inflammatory polarization of macrophages in visceral adipose tissue. When we performed core analysis of dysregulated miRNAs and transcripts in ATMs during diet-induced obesity, we found significant overlap with cardiometabolic disease processes and cancer, which suggests that ATM inflammation is tightly linked to the development of comorbid diseases.

Recent reports have linked specific miRNAs to obesity as well as macrophage polarization. In the context of obesity, expression profiles of human adipose tissue have identified miRNAs such as miR-132 and miR-17-5p to be involved in regulation of adipocyte growth and insulin resistance [34]. In macrophage polarization, miR-146a and miR-155-5p are classified to be negative regulators of inflammatory responses to the bacterial endotoxin lipopolysaccharide [35]. MicroRNA expression profiles of whole adipose tissue and in vitro polarized macrophages have been previously reported; however, dysregulated miRNAs between lean and obese ATMs have not been characterized [19, 34, 36]. ATMs form heterogenous populations and their inflammatory status greatly influences adipose insulin sensitivity. In the current study, the miRNAs that exhibited the most significant FC in ATMs were miR-322-5p and miR-155-5p. miR-322-5p is well characterized to inhibit pro-inflammatory cytokine production in macrophages, while miR-155-5p is also known to be involved in a variety of macrophage processes [28, 29]. Most strikingly, we observed downregulation of several miR-30 family miRNAs in ATMs during obesity, yet this miR family has not been previously investigated for its role regulating macrophage phenotype. The miR-30 family is highly conserved

and known to target the Notch1 ligand DLL4, which is a ligand that contributes to metabolic disease and macrophage inflammation [9, 30–33, 37]. We observed upregulation of DLL4 on obese ATMs. Moreover, inhibiting miR-30 in vitro triggered DLL4–Notch1 signaling and proinflammatory response in macrophages, and blocking DLL4–Notch1 signaling could lessen this effect. Overexpression of miR-30a-5p also decreased M1 polarization in the RAW264.7 macrophage cell line. Thus we have observed that miR-30 is involved in attenuating M1 macrophage activation through regulation of the DLL4–Notch signaling pathway. These data suggest that miR-30 induction holds therapeutic potential for regulating macrophage-driven inflammatory and metabolic disorders. Furthermore, regulatory mechanisms of the miR-30 family warrant further investigation due to emerging advances in epigenetic therapies and targeted personalized medicine.

To investigate the mechanisms through which obesity downregulates miR-30 in ATMs, we focused on epigenetic regulation. We observed elevated expression of DNMTs and DNA hypermethylation in miR-30-associated CpG islands in obese vs. lean ATMs. Thus HFD may trigger DNA hypermethylation of miR-30 genes leading to downregulation of miR-30 to allow increased expression of DLL4 and Notch signaling-induced inflammation and insulin resistance during obesity.

Previous studies have suggested that miR-30 induction has metabolic benefits. MicroRNA-30c attenuates hyperlipidemia, hypercholesterolemia, and atherosclerosis in mice, while miR-30b/c promotes thermogenesis and white adipose tissue browning [38–40]. These findings suggest that in vivo manipulation of the miR-30 family holds promise for therapeutic intervention of obesity-related disorders. Additionally, macrophage polarization plays key roles in regulation of both brown adipose tissue metabolism and inflammation during atherosclerosis, yet macrophage phenotype was not assessed in the aforementioned studies [41–43]. Our data suggest that macrophage-specific miR-30 regulates polarization toward inflammatory phenotype and progression of chronic macrophage-driven inflammatory disorders. Thus future studies targeting macrophage-specific miR-30 in vivo could shed new light on mechanistic and therapeutic potential of this miR family in attenuating obesity and other metabolic disorders.

Data and material availability

The data discussed in this publication have been deposited in NCBI's Gene Expression Omnibus and are accessible through GEO Series accession numbers GSE114735, GSE114736, and GSE114792 (https://www.ncbi.nlm.nih.gov/geo/query/acc.cgi?acc=GSE114735) (https://www.ncbi.nlm.nih.gov/geo/query/acc.cgi?acc=GSE114736) (https://www.ncbi.nlm.nih.gov/geo/query/acc.cgi?acc=GSE114792) [44].

Compliance with ethical standards

Conflict of interest The authors declare that they have no conflict of interest.

References

1. Hamilton TA, Zhao C, Pavicic PG, Datta S. Myeloid colony-stimulating factors as regulators of macrophage polarization. Front Immunol. 2014;5:554.
2. Boutens L, Stienstra R. Adipose tissue macrophages: going off track during obesity. Diabetologia. 2016;59:879–94.
3. Lumeng CN, Bodzin JL, Saltiel AR. Obesity induces. phenotypic switch in adipose tissue macrophage polarization. J. Clin Invest. 2007;117:175–84.
4. Bi P, Kuang S. Notch signaling as. novel regulator of metabolism. Trends Endocrinol Metab. 2015;26:248–55.
5. Borggrefe T, Liefke R. Fine-tuning of the intracellular canonical Notch signaling pathway. Cell Cycle. 2012;11:264–76.
6. Bi P, Shan T, Liu W, Yue F, Yang X, Liang X-R, et al. Inhibition of Notch signaling promotes browning of white adipose tissue and ameliorates obesity. Nat Med. 2014;20:911–8.
7. Pajvani UB, Shawber CJ, Samuel VT, Birkenfeld AL, Shulman GI, Kitajewski J, et al. Inhibition of Notch signaling ameliorates insulin resistance in. FoxO1-dependent manner. Nat Med. 2011;17:961–7.
8. Xu H, Zhu J, Smith S, Foldi J, Zhao B, Chung AY, et al. Notch-RBP-J signaling regulates the transcription factor IRF8 to promote inflammatory macrophage polarization. Nat Immunol. 2012;13:642–50.
9. Fukuda D, Aikawa E, Swirski FK, Novobrantseva TI, Koteliansky V, Gorgun CZ, et al. Notch ligand delta-like. blockade attenuates atherosclerosis and metabolic disorders. Proc Natl Acad Sci USA. 2012;109:E1868–1877.
10. Bam M, Yang X, Zumbrun EE, Zhong Y, Zhou J, Ginsberg JP, et al. Dysregulated immune system networks in war veterans with PTSD is an outcome of altered miRNA expression and DNA methylation. Sci Rep. 2016;6:31209.
11. Busbee PB, Nagarkatti M, Nagarkatti PS. Natural indoles, indole-3-carbinol (I3C) and 3,3'-diindolylmethane (DIM), attenuate staphylococcal enterotoxin B-mediated liver injury by downregulating miR-31 expression and promoting caspase-2-mediated apoptosis. PLoS ONE. 2015;10:e0118506.
12. Guan H, Singh UP, Rao R, Mrelashvili D, Sen S, Hao H, et al. Inverse correlation of expression of microRNA-140-5p with

progression of multiple sclerosis and differentiation of encephalitogenic. helper type 1 cells. Immunology. 2016;147:488–98.

13. Singh UP, Murphy AE, Enos RT, Shamran HA, Singh NP, Guan H, et al. miR-155 deficiency protects mice from experimental colitis by reducing. helper type 1/type 17 responses. Immunology. 2014;143:478–89.

14. Bartel DP. MicroRNAs: genomics, biogenesis, mechanism, and function. Cell. 2004;116:281–97.

15. Lewis BP, Burge CB, Bartel DP. Conserved seed pairing, often flanked by adenosines, indicates that thousands of human genes are microRNA targets. Cell. 2005;120:15–20.

16. Xiao C, Rajewsky K. MicroRNA control in the immune system: basic principles. Cell. 2009;136:26–36.

17. Dong C, Yoon W, Goldschmidt-Clermont PJ. DNA methylation and atherosclerosis. J. Nutr. 2002;132:2406S–2409S.

18. Zhang FF, Cardarelli R, Carroll J, Zhang S, Fulda KG, Gonzalez K, et al. Physical activity and global genomic DNA methylation in. cancer-free population. Epigenetics. 2011;6:293–9.

19. Ge Q, Brichard S, Yi X, Li Q. microRNAs as. new mechanism regulating adipose tissue inflammation in obesity and as. novel therapeutic strategy in the metabolic syndrome. J. Immunol Res. 2014;2014:987285

20. Xu H, Barnes GT, Yang Q, Tan G, Yang D, Chou CJ, et al. Chronic inflammation in fat plays. crucial role in the development of obesity-related insulin resistance. J. Clin Invest. 2003;112:1821–30.

21. Sturn A, Quackenbush J, Trajanoski Z. Genesis: cluster analysis of microarray data. Bioinformatics. 2002;18:207–8.

22. Bam M, Yang X, Zhou J, Ginsberg JP, Leyden Q, Nagarkatti PS, et al. Evidence for epigenetic regulation of pro-inflammatory cytokines, interleukin-12 and interferon gamma, in peripheral blood mononuclear cells from PTSD patients. J. Neuroimmune Pharmacol. 2015;11:168–81.

23. Lienhard M, Grimm C, Morkel M, Herwig R, Chavez L. MEDIPS: genome-wide differential coverage analysis of sequencing data derived from DNA enrichment experiments. Bioinformatics. 2014;30:284–6.

24. Freese NH, Norris DC, Loraine AE. Integrated genome browser: visual analytics platform for genomics. Bioinformatics. 2016;32:2089–95.

25. Kent WJ, Sugnet CW, Furey TS, Roskin KM, Pringle TH, Zahler AM, et al. The human genome browser at UCSC. Genome Res. 2002;12:996–1006.

26. Liao X, Sharma N, Kapadia F, Zhou G, Lu Y, Hong H, et al. Krüppel-like factor. regulates macrophage polarization. J. Clin Invest. 2011;121:2736–49.

27. van Stijn CMW, Kim J, Lusis AJ, Barish GD, Tangirala RK. Macrophage polarization phenotype regulates adiponectin receptor expression and adiponectin anti-inflammatory response. FASEB J. 2015;29:636–49.

28. O'Connell RM, Taganov KD, Boldin MP, Cheng G, Baltimore D. MicroRNA-155 is induced during the macrophage inflammatory response. Proc Natl Acad Sci USA. 2007;104:1604–9.

29. Zhang K, Song F, Lu X, Chen W, Huang C, Li L, et al. MicroRNA-322 inhibits inflammatory cytokine expression and

promotes cell proliferation in LPS-stimulated murine macrophages by targeting NF-κB1 (p50). Biosci Rep. 2017;37: BSR20160239.

30. Bridge G, Monteiro R, Henderson S, Emuss V, Lagos D, Georgopoulou D, et al. The microRNA-30 family targets *DLL4* to modulate endothelial cell behavior during angiogenesis. Blood. 2012;120:5063–72.

31. Shan T-D, Ouyang H, Yu T, Li J-Y, Huang C-Z, Yang H-S, et al. miRNA-30e regulates abnormal differentiation of small intestinal epithelial cells in diabetic mice by downregulating Dll4 expression. Cell Prolif. 2016;49:102–14.

32. Fung E, Tang S-MT, Canner JP, Morishige K, Arboleda-Velasquez JF, Cardoso AA, et al. Delta-like. induces Notch signaling in macrophages. Circulation. 2007;115:2948–56.

33. Nakano T, Fukuda D, Koga J, Aikawa M. Delta-like ligand 4-Notch signaling in macrophage activation. Arterioscler Thromb Vasc Biol. 2016;36:2038–47.

34. Klöting N, Berthold S, Kovacs P, Schön MR, Fasshauer M, Ruschke K, et al. MicroRNA expression in human omental and subcutaneous adipose tissue. PLoS ONE. 2009;4:e4699.

35. Taganov KD, Boldin MP, Chang K-J, Baltimore D, NF-κB-dependent induction of microRNA miR-146, an inhibitor targeted to signaling proteins of innate immune responses. PNAS. 2006;103:12481–6.

36. Zhang Y, Zhang M, Zhong M, Suo Q, Lv K. Expression profiles of miRNAs in polarized macrophages. Int. Mol Med. 2013;31:797–802.

37. Fukuda D, Aikawa M. Expanding role of delta-like. mediated notch signaling in cardiovascular and metabolic diseases. Circ J. 2013;77:2462–8.

38. Hu F, Wang M, Xiao T, Yin B, He L, Meng W, et al. miR-30 promotes thermogenesis and the development of beige fat by targeting RIP140. Diabetes. 2015;64:2056–68.

39. Soh J, Iqbal J, Queiroz J, Fernandez-Hernando C, Hussain MM. MicroRNA-30c reduces hyperlipidemia and atherosclerosis in mice by decreasing lipid synthesis and lipoprotein secretion. Nat Med. 2013;19:892–900.

40. Irani S, Pan X, Peck BCE, Iqbal J, Sethupathy P, Hussain MM. MicroRNA-30c mimic mitigates hypercholesterolemia and atherosclerosis in mice. J. Biol Chem. 2016;291:18397–409.

41. Moore KJ, Sheedy FJ, Fisher EA. Macrophages in atherosclerosis:. dynamic balance. Nat Rev Immunol. 2013;13:709–21.

42. Qiu Y, Nguyen KD, Odegaard JI, Cui X, Tian X, Locksley RM, et al. Eosinophils and type. cytokine signaling in macrophages orchestrate development of functional beige fat. Cell. 2014;157:1292–308.

43. Rao RR, Long JZ, White JP, Svensson KJ, Lou J, Lokurkar I, et al. Meteorin-like is. hormone that regulates immune-adipose interactions to increase beige fat thermogenesis. Cell. 2014;157:1279–91.

44. Edgar R, Domrachev M, Lash AE. Gene Expression Omnibus: NCBI gene expression and hybridization array data repository Nucleic Acids Res. 2002 Jan 1;30(1):207-10.